Stewart Ryan D. (Orcid ID: 0000-0002-9700-0351)

Bhaskar Aditi S. (Orcid ID: 0000-0001-9803-4003)

Herrmann Dustin L. (Orcid ID: 0000-0002-4227-8196)

Schifman Laura A. (Orcid ID: 0000-0003-4700-5530)

An analytical approach to ascertain saturation-excess versus infiltration-excess overland flow in urban and reference landscapes

Ryan D. Stewart[1*], Aditi S. Bhaskar[2], Anthony J. Parolari[3], Dustin L. Herrmann[4], Jinshi Jian[1,5], Laura A. Schifman[6], William D. Shuster[7]

[1]*School of Plant and Environmental Sciences, Virginia Polytechnic Institute and State University, Blacksburg, VA, United States.*

[2]*Department of Civil and Environmental Engineering, Colorado State University, Fort Collins, CO, United States.*

[3]*Department of Civil, Construction, and Environmental Engineering, Marquette University, Milwaukee, WI, United States.*

[4]*Oak Ridge Institute for Science and Education Research Participant Program with U.S. Environmental Protection Agency, Cincinnati, OH, United States.*

[5]*Joint Global Change Research Institute, Pacific Northwest National Laboratory, College Park, MD, United States.*

[6]*Department of Biology, Boston University, Boston, MA, United States.*

[7]*United States Environmental Protection Agency, Office of Research and Development, National Risk Management Research Laboratory, Cincinnati, OH, United States.*

This article has been accepted for publication and undergone full peer review but has not been through the copyediting, typesetting, pagination and proofreading process which may lead to differences between this version and the Version of Record. Please cite this article as doi: 10.1002/hyp.13562

*corresponding author: rds@vt.edu

Key Points

- Analytical model identifies propensity of one-dimensional soil profiles for saturation-excess vs. infiltration-excess overland flow
- Model estimates time and depth of overland flow based on soil profile properties
- Model quantified hydrologic functioning of pervious urban areas in 11 U.S. cities compared to pre-development reference conditions

Abstract

Uncontrolled overland flow drives flooding, erosion, and contaminant transport, with the severity of these outcomes often amplified in urban areas. In pervious media such as urban soils, overland flow is initiated via either infiltration-excess (where precipitation rate exceeds infiltration capacity) or saturation-excess (when precipitation volume exceeds soil profile storage) mechanisms. These processes call for different management strategies, making it important for municipalities to discern between them. In this study, we derived a generalized one-dimensional model that distinguishes between infiltration-excess overland flow (IEOF) and saturation-excess overland flow (SEOF) using Green-Ampt infiltration concepts. Next, we applied this model to estimate overland flow generation from pervious areas in eleven U.S. cities. We used rainfall forcing that represented low- and high-intensity events and compared responses among measured urban versus pre-development reference soil hydraulic properties. The derivation showed that the propensity for IEOF versus SEOF is related to the equivalence between two non-dimensional ratios: 1) precipitation rate to depth-weighted hydraulic conductivity, and 2) depth of soil profile restrictive layer to soil capillary potential. Across all cities, reference soil profiles were associated with greater IEOF for the high-intensity set of storms, and urbanized soil profiles tended toward production of SEOF during the lower-intensity set of storms. Urban soils produced more cumulative overland flow as a fraction of cumulative precipitation than reference soils, particularly under conditions associated with SEOF. These results will assist cities in identifying the type and extent of interventions needed to manage stormwater produced from pervious areas.

Keywords: urban hydrology; infiltration; urban soil; stormwater runoff

List of variables

θ_i – Initial water content [L^3 L^{-3}]

θ_s – Saturated water content [L^3 L^{-3}]

θ_r – Residual water content [L^3 L^{-3}]

α – van Genuchten (1980) water retention model parameter [L^{-1}]

m – van Genuchten (1980) water retention model parameter [-]

n_e – Available soil pore volume [L^3 L^{-3}]

Z – Depth to impermeable soil layer or water table [L]

$d\Psi/dz$ – Hydraulic gradient [L L^{-1}]

h_f – Wetting front potential [L]

z – Depth of wetting front beneath soil surface [L]

I – Cumulative infiltration [L]

q – Infiltration rate [L T^{-1}]

K_s – Saturated hydraulic conductivity [L T^{-1}]

r – Precipitation rate [L T^{-1}]

R – Cumulative precipitation [L]

t – Time since beginning of precipitation event [T]

t_p – Time to ponding due to infiltration-excess [T]

t_s – Time to ponding due to saturation-excess [T]

τ – Non-dimensional time, $\tau = K_s t / n_e h_f$ [-]

OF – Cumulative overland flow [L]

Γ – Non-dimensional overland flow, $\Gamma = OF/n_e h_f$ [-]

A – Constant in infiltration model, assumed to equal 2/3

B – Constant in infiltration model, assumed to equal 5/8

a – Parameter for runoff ratio (OF/R) model [-]

b – Parameter for runoff ratio (OF/R) model [-]

n – Number of soil profiles

D_i – Thickness of soil layer i [L]

Introduction

Overland flow, in which water supplied by precipitation or irrigation ponds on the soil surface and then runs off under the force of gravity, causes erosion, rapid contaminant transport, and flooding. The negative consequences of excess overland flow can be particularly acute in urban areas, where impervious cover minimizes infiltration (Leopold, 1968; Baruch *et al.*, 2018). With increases in urbanization, changes in frequency and intensity of precipitation patterns (Niyogi *et al.*, 2017), and the need to design more socially and ecologically sustainable cities (Tzoulas *et al.*, 2007), many urban areas are adding green spaces and green infrastructure (Gill *et al.*, 2007; Schifman *et al.*, 2017). These spaces are intended to reduce the amount of stormwater runoff entering already overwhelmed sewer systems, in part by relying on soils to infiltrate some of the overland flow generated from impervious surfaces (Voter and Loheide, 2018). However, pervious surfaces can also become sources of overland flow, indicating that such areas represent an important component of overall urban hydrologic response. Understanding the mechanisms and physical factors that determine overland flow generation from pervious surfaces is therefore necessary for quantifying the hydrologic impacts of urbanization.

Surface ponding and overland flow generation occurs via two principal mechanisms: infiltration-excess overland flow, hereafter IEOF, and saturation-excess overland flow, hereafter SEOF (Horton, 1933; Freeze, 1974). IEOF is initiated when the rate of water inputs (e.g., direct precipitation, irrigation, or overland flow routed to pervious areas as run-on) exceeds the infiltration rate of the soil. Under one-dimensional vertical flow conditions, infiltration rates typically diminish through time as the hydraulic gradient decreases towards unity, with the infiltration capacity of a soil asymptotically converging to field-saturated soil hydraulic conductivity (Philip, 1969). The rate at which infiltration capacity decreases is dynamic and interacts with soil capillarity (Stewart and Abou Najm, 2018) and wetting front depth (Green and Ampt, 1911; Selker and Assouline, 2017). By contrast, SEOF is a bottom-up process in the soil profile where moisture fills soil pores in an initially unsaturated volume above a hydraulically-restrictive soil layer, bedrock, or the water table (Dunne and Black, 1970; Loague *et al.*, 2010). If water inputs are sufficient to fill this pore volume, the soil profile becomes saturated and overland flow is initiated. The amount of available pore space is controlled by the initial water content and the depth of the soil profile, and these factors together provide the baseline from which saturated conditions develop.

Because of the different factors that drive IEOF and SEOF, most current analytical models do not include both processes and therefore poorly constrain the conditions and processes that favor IEOF versus SEOF in soil profiles. For example, urban runoff models like EPA-SWMM emphasize IEOF whereas rainfall-runoff models developed for forested catchments emphasize SEOF via the variable source area concept (McDonnell, 2003; Bartlett *et al.*, 2016). Recent discussions have emphasized that further conceptual refinement is needed (McDonnell, 2013), particularly to develop an analytical framework that represents SEOF and IEOF as linked processes. To date, however, there has been little progress towards this goal.

The ability to integrate SEOF and IEOF processes together becomes particularly important in urban settings, where heterogeneity in soil conditions and land cover increases the complexity of infiltration and saturation processes (Miles and Band, 2015; Lim, 2016).

While infiltration rates of urban soils are commonly analyzed as point measurements (Shuster *et al.*, 2014; Schifman and Shuster, 2018; Schifman *et al.*, 2018), a lack of understanding exists on which processes drive urban soils to generate runoff. The current paradigm in modeling runoff generation in urban catchments is that IEOF is the dominant overland flow generation process, because storm response in urban streams has been found to be closely related to the connectedness of impervious areas (Shuster *et al.*, 2005). Still, pervious areas also affect urban stormflow response, as permeable soils can mitigate the effect of urbanization on peak streamflow (Hopkins *et al.*, 2015; Smith and Smith, 2015). Urban development can also modify the soil profile via compaction (Batey, 2009; Shuster *et al.*, 2015), layering and changes in texture from backfilling, development of restrictive layers (Herrmann *et al.*, 2018), all of which can promote shallow or perched water tables and may increase the likelihood of SEOF. Such overland flow generation mechanisms have not been critically examined in these settings, either based on the current profile characteristics or on shifts that may have occurred in pervious urban areas compared to pre-development reference profiles. With cities turning towards increasing green or open spaces as part of their water management strategies, understanding propensity of urban soil to produce overland flow can guide the type and extent of stormwater runoff management intervention needed.

Rainfall characteristics also affect the type of stormwater runoff management intervention required (Figure 1). At the two extreme ends of the intensity-duration spectrum (i.e., low-intensity, short-duration events associated with the first flush of surface-located pollutants, and high-intensity, long-duration events associated with flood risks) overland flow generation has little relevance for management. Between these extremes, however, rainfall characteristics help determine whether a system will tend towards IEOF or SEOF. High intensity, short duration storms are most likely to result in runoff dominated by IEOF, as these events exceed the infiltration capacity of soils. In contrast, low intensity, long duration events are not anticipated to overwhelm infiltration capacity, but may saturate the available soil storage and result in surface runoff dominated by SEOF. Managing overland flow thus requires addressing multiple runoff pathways that are storm-dependent, and necessitates understanding such interactions between storm events and soils.

In this study, we test how soil profile characteristics and rainfall forcing affect whether runoff is generated by IEOF or SEOF, and then assess the influence of urbanization on runoff generation processes. To identify conditions under which IEOF or SEOF dominate runoff generation, the objectives of this study were threefold. For our first objective, we sought to develop an analytic framework that accounts for properties and processes that represent the propensity of a soil profile towards IEOF versus SEOF, based on a one-dimensional vertical treatment that characterizes when and how these mechanisms activate. Here we expected that low permeability soils (i.e., those with low values for saturated hydraulic conductivity) would be more prone to IEOF, while soils with shallow restrictive layers would be more prone to SEOF. For our second objective, we aimed to quantify the runoff ratio (overland flow as a fraction of precipitation) based on non-dimensional expressions for conditions under which IEOF and SEOF activate. For this objective we expected that overland flow initiation timing and amounts would vary between the IEOF and SEOF mechanisms. For our third objective, we worked to parameterize the analytical solutions and compare overland flow generation under relatively low- and high-intensity precipitation forcing using an urban and reference (pre-urban) dataset collected in 11 U.S. cities. Here we anticipated that urban soil profiles would generate more overland flow than reference soil profiles under both types of precipitation forcing.

Theory

Evaluating susceptibility to IEOF versus SEOF

To determine whether a soil profile will be more susceptible to infiltration-excess overland flow (IEOF) or saturation-excess overland flow (SEOF), we model a homogenous soil profile with a constant initial water content (θ_i [L^3 L^{-3}]) throughout the profile. We assume that the soil has an available soil pore volume, n_e [L^3 L^{-3}], where $n_e = \theta_s - \theta_i$, that the saturated water content θ_s [L^3 L^{-3}] represents the maximum amount of wetting in the unsaturated zone, and that this pore volume sits above an impermeable restrictive layer or water table located at a depth Z [L] from the surface.

We estimate the time to IEOF, t_p [T], using the Green-Ampt infiltration model. The Green-Ampt model assumes that water infiltrates with a sharp wetting front along a hydraulic gradient characterized as $d\Psi/dz = (h_f + z)/z$, where h_f [L] is the wetting front potential, and z [L] is the depth of the wetting front beneath the soil surface and increases downward. The wetting front depth z is related to the cumulative infiltration, I [L], as $z = I/n_e$. Substituting this representation of hydraulic gradient into Darcy's law yields:

$$q = K_s\left(\frac{d\Psi}{dz}\right) = K_s\left(\frac{I + h_f n_e}{I}\right) \tag{1}$$

where q [L T^{-1}] is the infiltration rate and K_s [L T^{-1}] is the saturated hydraulic conductivity.

Selker and Assouline (2017) derived the following approximation to Equation (1), which implicitly accounts for cumulative infiltration I when calculating q:

$$q = K_s\left(1 + \frac{A + \sqrt{\frac{n_e h_f}{2K_s t}}}{1 + A\frac{K_s t}{n_e h_f} + \sqrt{\frac{2K_s t}{n_e h_f}}}\right) \qquad r > K_s \tag{2}$$

where A is a constant (typically taken to equal 2/3). As ponding will occur when the infiltration (q) and precipitation rates (r) are equal, the time to ponding (t_p) is found implicitly using Equation (2) as:

$$\frac{r}{K_s} = 1 + \frac{A + \sqrt{\frac{n_e h_f}{2K_s t_p}}}{1 + A\frac{K_s t_p}{n_e h_f} + \sqrt{\frac{2K_s t_p}{n_e h_f}}} \qquad r > K_s \qquad (3).$$

We take advantage of the the following explicit, approximated expression for time to ponding (discussed further in Appendix A):

$$t_p = \left(\frac{h_f n_e}{r/K_s - 1}\right)\left(\frac{B}{r}\right) \qquad r > K_s \qquad (4)$$

where B is a constant taken here to equal 5/8.

Next, the saturation-excess ponding condition will occur when the depth of infiltrated precipitation equals the depth of available storage in the profile:

$$I = rt_s = n_e Z \qquad (5)$$

where t_s [T] represents the time to SEOF. Rearranging Equation (5):

$$t_s = n_e Z / r \qquad (6).$$

SEOF will precede IEOF whenever $t_s < t_p$, so combining that inequality with Equations (4) and (6) gives:

$$\frac{Z}{h_f} < \left(\frac{B}{r/K_s - 1}\right) \qquad r > K_s \qquad (7).$$

Simulating overland flow depths under IEOF versus SEOF

As a precursor to quantifying runoff ratio, we first develop expressions for depth of overland flow *OF* [L] at time *t* [T] for both IEOF and SEOF scenarios. We start by assuming that *OF* is equal to the precipitation depth minus the cumulative infiltration, i.e., $OF = rt - I$.

In the IEOF case, we normalize Equation (4) as:

$$q = K_s\left(1 + \frac{A + \sqrt{\frac{1}{2\tau}}}{1 + A\tau + \sqrt{2\tau}}\right) \quad \square \; r > K_s \qquad (8)$$

where τ is a non-dimensional form of time (Fok, 1975; Stewart, 2019):

$$\tau = \frac{K_s t}{n_e h_f} \qquad (9a)$$

$$\tau_p = \frac{K_s t_p}{n_e h_f} \qquad (9b)$$

In normalized time, infiltration rate *q*, and the cumulative infiltration, *I*, are related:

$$I = \int q dt = \frac{n_e h_f}{K_s}\int q d\tau \qquad (10).$$

The non-dimensional time to ponding is found implicitly as:

$$\frac{r}{K_s} = 1 + \frac{A + \sqrt{1/2\tau_p}}{1 + A\tau_p + \sqrt{2\tau_p}} \qquad (11),$$

noting that Equation (4) can also be used as an explict estimation of time to ponding, with some minor error.

Once the soil ponds, the depth of cumulative infiltration into the matrix will be found by:

$$I = n_e h_f \left(\frac{r}{K_s}\right)\tau_p + \frac{n_e h_f}{K_s}\int_{\tau_p}^{\tau} q(\tau')d\tau' \qquad \tau \geq \tau_p;\ r > K_s \tag{12}$$

where τ' is a dummy variable of integration. Integrating Equation (12) using Equation (10) results in:

$$I = n_e h_f \left[\left(\frac{r}{K_s} - 1\right)\tau_p + \tau + \ln\left(\frac{1 + A\tau + \sqrt{2\tau}}{1 + A\tau_p + \sqrt{2\tau_p}}\right)\right] \qquad \tau \geq \tau_p;\ r > K_s \tag{13}$$

Using Equation (13), we can express *OF* as:

$$OF = n_e h_f \left[\left(\frac{r}{K_s} - 1\right)\left(\tau - \tau_p\right) - \ln\left(\frac{1 + A\tau + \sqrt{2\tau}}{1 + A\tau_p + \sqrt{2\tau_p}}\right)\right] \qquad \tau \geq \tau_p;\ r > K_s \tag{14}$$

Equation (14) can also be expressed as a non-dimensional quantity using:

$$\Gamma = \left(\frac{r}{K_s} - 1\right)\left(\tau - \tau_p\right) - \ln\left(\frac{1 + A\tau + \sqrt{2\tau}}{1 + A\tau_p + \sqrt{2\tau_p}}\right) \qquad \tau \geq \tau_p;\ r > K_s \tag{15}$$

where $\Gamma = OF/n_e h_f$.

For SEOF, the non-dimensional time to saturation (τ_s) is:

$$\tau_s = \frac{Z / h_f}{r / K_s} \tag{16}$$

Overland flow (*OF*) can be calculated for SEOF as $rt - n_e Z$, or in non-dimensional time as:

$$OF = n_e h_f \frac{r}{K_s}\left(\tau - \tau_s\right)$$ □ $\tau \geq \tau_s$ (17).

$$\Gamma = \frac{r}{K_s}\left(\tau - \tau_s\right)$$ □ $\tau \geq \tau_s$ (18).

Runoff ratio quantification

We next quantify runoff ratio (i.e., *OF/R*) for either runoff generation process, using the non-dimensional relationship r/K_s that was described in the previous derivation. For IEOF, starting with Equation (14) and $R = rt$, the runoff ratio can be expressed as a function of r/K_s:

$$\frac{OF}{R} = \frac{\tau - \tau_p}{\tau}\left\{1 - \left[1 + \frac{\tau}{\tau - \tau_p}\ln\left(\frac{1 + A\tau + \sqrt{2\tau}}{1 + A\tau_p + \sqrt{2\tau_p}}\right)\right]\left(\frac{r}{K_s}\right)^{-1}\right\}$$ □ $\tau \geq \tau_p$ (19).

Similarly, using Equation (17) to derive the runoff ratio for SEOF:

$$\frac{OF}{R} = 1 - \frac{\tau_s}{\tau} = 1 - \left(\frac{Z}{h_f \tau}\right)\left(\frac{r}{K_s}\right)^{-1}$$ □ $\tau \geq \tau_s$ (20).

Both relationships (19) and (20) have the general form:

$$\frac{OF}{R} = a\left[1 - b\left(\frac{r}{K_s}\right)^{-1}\right]$$ (21)

with the parameters *a* and *b* for IEOF and SEOF given in Table 1. When both *a* and *b* are unity, our derivation indicates a steep rise in runoff ratio as the ratio r/K_s exceeds 1 (e.g., when the precipitation rate starts to exceed the hydraulic conductivity of the near-surface soil).

Methods

Field data

Urban soil profiles were assessed in eleven cities across the United States: A = Atlanta, GA (number of soil profiles n = 15); C = Camden, NJ (n = 28); D = Detroit, MI (n = 57); I = Cincinnati, OH (n = 67); J = San Juan, PR (n = 26); N = New Orleans, LA (n = 19); O = Omaha, NE (n = 36); P = Portland, ME (n = 67); T = Tacoma, WA (n = 17); V = Cleveland, OH (n = 127); X = Phoenix, AZ (n = 13). Infiltration rates were measured at the surface using a tension infiltrometer (Mini-disk tension infiltrometer; METER Group, Pullman, USA) with source pressure head h_s = -2 cm. Measured data were used as a proxy for saturated hydraulic conductivity (K_s) following the method of Zhang (1997). Subsurface infiltration rates were measured using a borehole permeameter; and the Glover solution (Zangar, 1953) was used to infer K_s from those data. For each urban profile, a corresponding reference (i.e., pre-development) soil profile was developed as in Herrmann *et al.* (2018), which involved expert input from USDA-NRCS soil scientists with knowledge specific to each city.

Model parameterization

In the urban profiles, Z was constrained by the depth of the first hydraulically restrictive layer that was field-identified as restrictive with the presence of fragipans (i.e., dense layers that restrict water movement and root growth), the presence of redoximorphic features as an indication of seasonal water table development, abrupt shift to soil horizon with finer texture, or $K_s < 0.1$ cm h^{-1} (Thomas *et al.*, 2016). If no restrictive layers were observed, Z was set as the bottom of the lowest soil layer assessed. For the reference profiles, Z was also set at the top of any restrictive layer (i.e., $K_s < 0.1$ cm h^{-1}), or the bottom of lowest reported layer. To estimate other soil hydraulic properties, we used the measured % sand, silt, and clay data, along with any reported data (e.g., bulk densities for both urban and reference profiles; water retention data for reference profiles). These data were input into random forest pedotransfer function (PTF) models that were trained to provide values for the van Genuchten (1980) water retention parameters θ_r, θ_s, α, and m, along with K_s for any soil layer in which that property had not been measured directly via field assessments. More information on the PTF functions is provided in Appendix B.

Individual layer K_s values were compiled into a single representative K_s for each profile using the technique described by Oosterbaan and Nijland (1994):

$$K_s = Z \Big/ \sum_{i=1}^{n} D_i / K_{s,i} \tag{22}$$

where D is the thickness of each layer i.

Likewise, individual layer θ_s values were compiled into a single depth-weighted θ_s for each profile by:

$$\theta_s = \frac{1}{Z} \sum_{i=1}^{n} \theta_{s,i} D_i \tag{23}$$

.

To simulate similar conditions across cities, the available pore space n_e for the profile was assumed to equal $0.75\theta_s$. This value represented moderately dry initial conditions that still included some antecedent moisture.

The wetting front potential h_f was estimated using the following equation (Morel-Seytoux *et al.*, 1996):

$$h_f = \left(\frac{1}{\alpha}\right)\left(\frac{0.046m + 2.07m^2 + 19.5m^3}{1 + 4.7m + 16m^2}\right) \quad (24)$$

where α and m represent the van Genuchten water retention parameters. We used the surface layer h_f value to represent the entire profile.

Values of Z/h_f and r/K_s were then calculated for each soil profile, with K_s estimated by Equation (22). Individual soil profiles were then aggregated to provide per-city means and errors for K_s, h_f, Z, and n_e; K_s was calculated as a geometric mean with 95% confidence intervals, while h_f, Z and n_e were calculated as arithmetic means along with standard errors of the means.

Next, simulations for each profile were forced with 2-year recurrence interval storms of 1- and 24-hour durations, with storms calculated for each individual city (Miller *et al.*, 1973; Bonnin *et al.*, 2006). The precipitation durations (i.e., 1 and 24 h) were normalized as τ using Equation (9) along with estimated K_s, h_f, and n_e values for each soil profile. The mean precipitation rates r [L T^{-1}] were calculated as total precipitation R [L] divided by duration t [T]. The times to ponding and saturation were also calculated for each combination of soil profile and precipitation intensity using Equations (11) and (16). Whenever $\tau < \tau_p < \tau_s$, overland flow depths OF and Γ were calculated using Equations (14) and (15); whenever $\tau < \tau_s < \tau_p$, overland flow depths were calculated using Equations (17) and (18). Runoff ratios were calculated for each location and event as total overland flow OF over cumulative precipitation R, and according to Equations (19) and (20). To assess the potential influence of urbanization on soil properties and overland flow depths, we compared per-city values of $\ln(K_s)$, h_f, Z, n_e, and OF (from the 1- and 24-hour storms) between urban and reference profiles using pairwise t-tests (α = 0.05).

Results

Susceptibility to IEOF versus SEOF

Using our model framework, we found that IEOF and SEOF occurrence is differentiated by the behavior of two non-dimensional variables: precipitation rate normalized to hydraulic conductivity, r/K_s, and soil depth normalized to wetting front potential, Z/h_f. Figure 2 shows the theoretical propensity for IEOF compared to SEOF, as estimated by Equation (7). Conditions where the precipitation rate r far exceeds K_s lead to greater IEOF propensity, whereas SEOF is the only possible runoff generation mechanism if r is less than K_s. If the depth of the soil profile Z is much smaller than wetting front potential h_f, SEOF can occur even when r/K_s is greater than 1. A shallower soil profile (smaller Z) takes less water to saturate completely, while a large wetting front potential drives a greater initial infiltration rate, reducing the propensity for IEOF and increasing that for SEOF.

After overland flow is initiated by IEOF or SEOF, the model simulates the accumulation of non-dimensional overland flow (Γ; Equations 15 and 18) over time in a way that depends both on the runoff generation mechanism and r/K_s. Our derivation relied on shifting to a non-dimensional time frame, which showed that the rate of overland flow increases through time for IEOF (Figure 3a) while remaining linear for SEOF (Figure 3b). As values of r/K_s increase, overland flow depth accumulates faster for both IEOF and SEOF, but overland flow depth accumulates in different ways for IEOF and SEOF. For IEOF, when precipitation rate nominally exceeds hydraulic conductivity ($r/K_s = 1.2$), overland flow accumulates more slowly, and to a smaller cumulative depth, than when r/K_s is larger.

Reference and urban soil profile properties

Next, we investigated the soil characteristics in reference and urban soil profiles. For most cities (i.e., Atlanta, Detroit, Cincinnati, Cleveland, Omaha, Portland, Tacoma), the geometric mean of depth-weighted K_s values was lower for urban than reference profiles (Figure 4a), though the differences were not significant for Atlanta, Cincinnati, or Omaha (paired t-test; $p \geq 0.05$). For other cities (i.e., Camden, San Juan, New Orleans, Phoenix) the mean reference K_s was lower than the urban mean K_s, although the difference was not significant for Camden (paired t-test; $p \geq 0.05$). The wetting front potential was generally higher in urban soil profiles compared to reference profiles (Figure 4b), though San Juan, New Orleans and Tacoma all had significantly smaller h_f values in the urban profiles (paired t-tests; $p < 0.05$). Six of the cities (Atlanta, New Orleans, Omaha, Portland, Tacoma and Cleveland) had shallower depths to restrictive layers (Z) when urbanized (Figure 4c). In four of the cities (Atlanta, Camden, Omaha, and Phoenix), Z was constrained for the reference profiles by the limit of collected data, and in reality may have extended even deeper than reported, as the urban profile depths for Camden and Omaha both had depths of more than 250 cm. For most cities, the available pore space was lower in urban soil profiles than reference profiles, though differences were minor: overall mean $n_e = 0.341$ in the reference profiles and $n_e = 0.324$ in the urban profiles (data not shown).

Urbanization effects on susceptibility to IEOF versus SEOF

The non-dimensional hydraulic characteristics Z/h_f (depth normalized wetting front potential) and r/K_s (relative precipitation rate) were compiled for the 11 cities. Here, city-specific precipitation rates were quantified for 1-hour and 24-hour durations based on a 2-year return period (Figure 5). For all soils and both precipitation durations, the propensity towards IEOF or SEOF (as modeled by Equation 7) was more strongly controlled by the relative precipitation rate (r/K_s) than the depth-normalized wetting front potential (Z/h_f). With the 1-hour duration, nearly all reference and urban soils were estimated to experience IEOF before SEOF (Figure 5a). The exceptions were Tacoma, which even under the higher 1-hour precipitation intensity exhibited a tendency towards SEOF in both urban and reference conditions, and the reference profiles in Portland. For the 24-hour duration, SEOF was estimated to be the most likely runoff generation mechanism (Figure 5b). Here, the two exceptions were the reference profiles from San Juan and New Orleans, which, due to relatively low K_s values (Figure 4a), were still more likely to produce surface runoff via IEOF.

At the level of individual soil profiles, changes imposed by urbanization also altered both the type and the magnitude of runoff generation for different storm intensities and durations (Figure 6). For the 1-hour, 2-year set of storms, urbanization caused a mixed response in terms of the total proportion of profiles that produced overland flow via combined IEOF and SEOF. In Atlanta, Camden, Tacoma, and Cleveland, more profiles produced overland flow after urbanization compare to the reference profiles, whereas Cincinnati, New Orleans, Omaha, Portland, and Phoenix had the opposite response (Figure 6a, b). Detroit and San Juan had no change for this particular set of storm events. Most profiles, whether urban or reference, produced surface runoff via IEOF, with only a small number of urban profiles in Atlanta and New Orleans producing SEOF. For the lower-intensity 24-hour, 2-year set of storms, urbanization not only increased the number of profiles that generated overland flow, but also increased the proportion of profiles that generated runoff by the SEOF mechanism (Figure 6c, d). Atlanta, Camden, San Juan, New Orleans and Cleveland all had the majority of overland flow produced via SEOF during this set of lower-intensity storms, due to shallow soil profiles (represented by small values of Z) found in those cities.

Urbanization effects on cumulative overland flow

The effects of urbanization on cumulative overland flow depended on precipitation intensity. Cumulative overland flow for the 1-hour, 2-year storms was either similar or higher in the reference soil profiles as compared to the urban soil profiles (Figure 7a). Specifically, Phoenix, Cincinnati, Camden, Omaha, San Juan and New Orleans all had higher estimated overland flow amounts in the pre-development reference state. While this finding can be explained by the higher K_s values estimated for the urban soils in Phoenix, Camden, San Juan and New Orleans (Figure 4a), the differences for Cincinnati and Omaha corresponded to larger h_f values in urban compared to reference profiles (Figure 4b).

By contrast, the reference soil profiles had equal or lower amounts of overland flow for the 24-hour 2-year storms, with the exceptions of San Juan and New Orleans, where the reference profiles still had greater overland flow depths compared to the urban ones (Figure 7b). Those two cities (San Juan and New Orleans) both had relatively high 24-hour 2-year precipitation amounts, and relatively low reference K_s values (Figure 4a). For the remaining profiles, urbanization was associated with smaller depth-normalized wetting front potential (i.e., smaller Z/h_f values; Figure 5), and therefore less time to saturation (Equation 16).

Urbanization effects on runoff ratio

The runoff ratio response (i.e., cumulative overland flow as a fraction of cumulative precipitation, OF/R) was similar in shape to that estimated by Equation (21) for different precipitation events (Figure 8). However, the use of actual field data for different soils detailed variability in how runoff ratio responds, especially with regard to the spread of data across the range of r/K_s. Under the set of 1-hour storms, most of the overland flow was attributed to infiltration-excess, and the urban and reference profiles had similar responses (Figure 8a). Under the lower intensity 24-hour storms, however, the runoff ratio varied substantially between reference and urban soil profiles (Figure 8b). Many urban soils produced more cumulative overland flow as a fraction of cumulative precipitation than reference soils. The differences were most pronounced for $r/K_s \leq 1$, which represents conditions associated with SEOF. For both sets of storms, certain soil profiles generated lower OF/R than estimated by Equation (21), primarily under IEOF conditions (i.e., $r/K_s > 1$).

These soil profiles were characterized by high h_f values, which meant that they could infiltrate relatively more water before ponding.

Discussion

An analytical model was developed to evaluate the propensity of soil profiles to produce surface runoff via infiltration-excess overland flow (IEOF) versus saturation-excess overland flow (SEOF). Three factors were important to this analysis: depth-averaged saturated hydraulic conductivity, K_s, wetting front potential, h_f, and depth to restrictive layer, Z. Small values of the first two parameters favored runoff generation via IEOF, while small values for Z favored SEOF (Figure 2).

The model was used to analyze how runoff initiation timing and amounts vary between overland flow processes. The results showed that, for a given precipitation rate, SEOF will accumulate overland flow more rapidly than for any IEOF scenario, because during IEOF some water will continue to infiltrate whereas all precipitation become overland flow during SEOF (Figure 3). Still, even though SEOF produces relatively more overland flow than IEOF after ponding or saturation occurs, the time to these conditions are not equivalent. For $r/K_s > 1$, unless Z is quite small or h_f is quite large, IEOF will begin earlier than SEOF (Figure 2). Thus, infiltration-excess can produce more overland flow than surface-excess, depending on specific storm and soil characteristics.

Next, the model was used to interpret how changes in soil profiles and hydraulic properties imposed by urbanization impact runoff generation mechanisms and overland flow depths (Figure 4). In the dataset described here, urbanization increased the propensity of SEOF during long-duration, low-intensity storms. However, in some cases urbanization ameliorated IEOF that can occur during high-intensity storm events. By casting the critical model parameters (K_s, h_f, Z) and precipitation rate (r) into two non-dimensional numbers, r/K_s

and Z/h_f, our analysis was able to place soil profiles for 11 cities as being initially susceptible to either SEOF or IEOF under two different storm intensities (Figures 5 and 6). The model was then used to explore overland flow amounts (Figure 7) and proportion of precipitation (Figure 8).

The results revealed a nuanced picture of the hydrologic changes that urbanization can induce. For instance, four of the cities were estimated to have increased K_s values in urban versus reference profiles, reflecting better ability to absorb precipitation. Likewise, seven of the cities had higher h_f values in the urban profiles, again indicating better infiltration capacity. However, the urban profiles had smaller Z values, signifying less storage in the profile before saturation. As a result of these shifts between urban and reference profile properties, many of the cities had less estimated overland flow during high intensity events (represented by 1-hour, 2-year storms) under urban compared to reference conditions. Under low intensity events, however, urban profiles tended to generate more overland flow than reference ones, due to saturation effects. As a result, urbanization appears to increase the range of conditions under which many soils will produce overland flow, even if the total accumulated depths may be reduced in certain locations (e.g., in New Orleans, LA and San Juan, PR which had relatively high urban K_s values; Figure 4) and under certain conditions (e.g., high intensity rains in Cincinnati, OH).

Our analysis focused only on identifying the initial overland flow generation mechanism that is likely to act on a soil profile. As a consequence, we assumed that a soil profile will respond to precipitation forcing by either SEOF or IEOF, but not both. Previous work has suggested that certain soils may experience both runoff generation mechanisms over the course of changing precipitation (Yang *et al.*, 2015). Our model could therefore under-estimate runoff generation in soils that were characterized as having IEOF runoff generation (i.e., $\tau_p < \tau_s$) if those soils were to saturate during the course of an event. Since the urban soils analyzed here were more likely to have small Z/h_f values, it is possible that overland flow was underestimated in some profiles, particularly for the 24-hour, 2-year events.

Here we note that our analysis obscured the role of available pore space, n_e, in overland flow processes. For one, in our analysis we assumed that the non-dimensional quantity developed to delineate IEOF and SEOF (i.e., Equation 7) is independent of available pore space n_e. While this result is valid for a uniform vertical distribution of available pore space (e.g., the uniformly distribution of $n_e = 0.75\theta_s$ we assumed), it will not hold true whenever available pore space varies with depth. As soil profiles often have increasing water content with depth, the solution posed here trades some realism in exchange for simplicity required from an analytical model. Our assumption of $n_e = 0.75\theta_s$ meant that the soils were treated as being fairly dry at the beginning of the event. This assumption likely minimized the potential effect of that term in actual overland flow generation, as both surface-excess and infiltration-excess overland flow will occur more rapidly in initially wet soils. We also assumed that the initial wetting front potential h_f can be treated as a constant with minimal effect on results, although in reality h_f will decrease as the initial water content increases (see Stewart *et al.* (2013) or Stewart and Abou Najm (2018) for more discussion of this point). Even so, under our assumption of 75% available pore space volume ($\theta_i > \sim 0.75\theta_s$), the wetting front potential can be approximated as a constant nearly equal to the maximum value found in completely dry soil.

We chose to use depth-averaged K_s values in our analysis (Equation 22) to better integrate changes throughout the soil profile that occurred during urbanization. This approach is valid for one-dimensional flow under conditions where the hydraulic gradient through each layer can adjust to maintain steady-state (and typically saturated) flow through different soil layers (Bos, 1994). If the surface/near-surface layer is the most hydraulically restrictive, however, this assumption may not be valid, as excess water can be removed via overland flow before the gradient adjusts. This discrepancy could result in under-estimates for overland flow in cases where the lowest K_s values occur at or near the surface. In the dataset tested here, 99 out of 472 urban profiles and 83 out of 472 reference profiles had surface K_s values that were less than half as large as the profile-weighted K_s values. However, only 4 of the urban profiles (and no reference profiles) had surface K_s values more than one order of magnitude smaller than the profile average. The uncertainty associated with this assumption should thus be small in this case, though additional scrutiny may be required in other applications.

The model also considered soils as simplified one-dimensional profiles, thus ignoring factors such as surface topography and landscape connectivity. In urban systems, run-on from impervious surfaces can contribute additional water to pervious surfaces. This additional flow may result in quicker saturation, which may impact the processes and timing at which point overland flow starts in comparison to reference landscapes (Voter and Loheide, 2018). Surface topography also can play an important role in runoff generation, both by altering the amount of infiltration that occurs in sloping versus flat surfaces (Chen and Young, 2006) and by increasing wetness in low-lying and convergent portions of the landscape (Zimmer and McGlynn, 2018). Still, the parameters identified here as being most important to runoff generation likely act as primary controls on overland flow in more complex settings.

Despite the aforementioned assumptions and simplifications, the model confers the ability to characterize most likely runoff generation mechanisms and captures differential responses induced by precipitation intensity versus duration (Dunkerley, 2016; Masselink *et al.*, 2016; Dunkerley, 2018). The model was developed using an original and comprehensive dataset collected in 11 cities across the U.S. The cities studied here varied widely in climate type (Kottek *et al.*, 2006), while the soil profiles included all twelve textures recognized by the USDA National Resoures Conservation Service (Soil Survey Staff, 2014) and possessed a range of soil properties (e.g., Z, h_f, K_s). These results are therefore likely to be representative of conditions found in many other urban areas around the world. At the same time, the model framework developed here should be applicable to any agency or municipality charged with urban water management.

In terms of specific intervention strategies, cities with urban soil profiles prone to IEOF could be best suited for interventions that increase infiltration capacity, thus maximizing the precipitation rate at which overland flow is initiated. Some strategies to augment infiltration rates include using refined demolition practices (U.S. E.P.A., 2013) or subsoiling (Schwartz and Smith, 2016), maintaining vegetation over the long-term to protect the soil surface and preserve organic matter content, and increasing surface roughness, so as to concomitantly promote infiltration and mitigate against overland flow formation. For SEOF, targeted management strategies could be to reduce the additional water inputs that could lead to saturation (impervious surfaces draining to pervious surfaces or urban landscape irrigation) while increasing available pore space in the soil profile or breaking up subsurface restrictive layers.

Our findings show that, for long-duration storms, SEOF is more common in urban soils than their pre-development reference counterparts, emphasizing the need to increase soil capacity for storing stormwater. At the same time, SEOF may be even more prevalent in urban soils than estimated here due to additional water that becomes delivered from adjacent impervious areas during storm events. Future climate projections also indicate a shift in precipitation regimes to less frequent storm events, but greater precipitation loads per event. If this shift results in a greater occurrence of low-intensity, long-duration storms, a focus on SEOF management will become increasingly appropriate for urban areas.

Summary and Conclusions

In this study we used Green-Ampt infiltration concepts in a non-dimensional framework to identify propensity towards infiltration-excess overland flow (IEOF) versus saturation-excess overland flow (SEOF). Overland flow generation type varied as a function of rainfall rate over depth-weighted hydraulic conductivity (r/K_s) versus depth of the soil profile restrictive layer to soil capillary potential (Z/h_f). Field measurements collected in 11 U.S. cities showed that, compared to the pre-development reference condition, urbanization often increased K_s and h_f, leading many of the cities to produce less surface runoff via IEOF. However, urbanization also led to shallower restrictive layer depths (Z), meaning that many cities may be more prone to SEOF during low-intensity, long-duration storms.

The model output presented here highlights runoff generation processes from direct catch inputs of precipitation. We developed and applied this model to urban areas, due to our ability to compare and contrast soil profiles and the open questions regarding the effects of urbanization on precipitation partitioning in pervious areas. Still, these concepts can apply to other systems in which overland flow is generated by both IEOF and SEOF. Some examples could be other non-forested landscapes where IEOF is important, such as those with little vegetative cover (e.g., burned watersheds, fallow agricultural areas, arid watersheds). Even though the approach does make a number of simplifications, such as assuming uniform and homogenous one-dimensional vertical profiles, it still allows assessment of the relative likelihood of two important runoff generation processes based on a few parameters that can be easily measured in the field.

This work could be complemented by field monitoring of conditions that lead to overland flow from urban pervious areas, and the correspondence of these field conditions to important parameters in the analytical model developed. A greater understanding of the conditions under which pervious urban areas can infiltrate water and the limiting factors to infiltration (whether this is soil depth or saturated hydraulic conductivity) could help inform urban water managers. An example application could be mapping areas such as lawns that can infiltrate additional water from disconnected downspouts versus those that may generate overland flow and contribute to flooding during storm events. Finally, the results presented here highlight that urbanization can induce distinct hydrological responses across cities, thus emphasizing the importance of having straight-forward analytical tools, such as the one presented here, when designing interventions.

Data Availability Statement

Data from this paper is permanently archived at https://data.lib.vt.edu/files/00000011h.

Acknowledgments

Funding for this work was provided in part by the Virginia Agricultural Experiment Station and the Hatch Program of the National Institute of Food and Agriculture, U.S. Department of Agriculture. The research was performed while D.L. Herrmann held a postdoctoral research participant appointment administered by the Oak Ridge Institute for Science and Education through Interagency Agreement No. DW-8992433001 between the U.S. Department of Energy and the U.S. Environmental Protection Agency (E.P.A.) at the National Risk Management Research Laboratory within the Office of Research and Development of the U.S. E.P.A. The views expressed in this paper are those of the authors and do not necessarily represent the views or policies of the U.S. E.P.A.

Appendix A

The Green-Ampt model states that:

$$q = K_s\left(\frac{d\Psi}{dz}\right) = K_s\left(\frac{I + h_f n_e}{I}\right) \tag{A1}$$

where q [L T^{-1}] is the infiltration rate, K_s [L T^{-1}] is the saturated hydraulic conductivity, $d\Psi/dz$ is the hydraulic gradient [L L^{-1}], h_f [L] is the wetting front potential, n_e is the available pore space, and I is the cumulative infiltration [L].

Ponding will occur when the infiltration rate matches the precipitation rate, r [L T^{-1}]; therefore, substituting $q = r$ into Equation (A1) and rearranging gives:

$$I_p = \frac{h_f n_e}{r/K_s - 1} \qquad □\ r > K_s \tag{A2}$$

where I_p [L] is the depth of infiltration at the time of ponding. Since $t_p = I_p/r$, Equation (A2) can be solved as:

$$\tau_p = \left(\frac{1}{r/K_s - 1}\right)\left(\frac{K_s}{r}\right) \qquad □\ r > K_s \tag{A3}$$

where $\tau_p = K_s t_p / n_e h_f$.

In the Selker and Assouline (2017) approximation, the normalized time to ponding (τ_p) is found implicitly by:

$$\frac{r}{K_s} = 1 + \frac{A + \sqrt{\frac{1}{2\tau_p}}}{1 + A\tau_p + \sqrt{2\tau_p}} \qquad □\ r > K_s \tag{A4}$$

The time to ponding τ_p values given by equations (A3) versus (A4) are not equivalent; however, by modifying equation (A3) with a parameter B we can obtain a “universal” approximation for time to ponding with the Green-Ampt family of models:

$$\tau_p = \left(\frac{1}{r/K_s - 1}\right)\left(B\frac{K_s}{r}\right) \qquad r > K_s \qquad \text{(A5).}$$

When B = 1, Equation (A5) becomes equal to Equation (A3), while when $B \approx 5/8$, the time to ponding τ_p values estimated by equations (A4) and (A5) become nearly identical (Figure A1). Therefore, we can use Equation (A5) with B = 5/8 to obtain a close explicit approximation for time of ponding when working with the Selker and Assouline (2017) expression.

Appendix B

We estimated missing values for K_s and the van Genuchten (1980) water retention parameters θ_r, θ_s, α, and m by developing pedotransfer functions (PTFs) using random forest modeling. The K_s model was trained using 711 observations collected in 12 cities (i.e., the 11 cities included in this study plus 9 urban profiles assessed in Majuro, Republic of the Marshall Islands). Of those 711 observations, 228 were from the reference profiles (each representing a unique record), using the K_s values reported in the National Cooperative Soil Survey database. The other 543 K_s values were measured in the urban profiles using either surface-placed tension infiltrometers or subsurface borehole tests. The model inputs were categorical soil texture or percent sand, silt, and clay, the latter selected when available (Figure B1). In total, the PTF models were used to estimate K_s for 1790 urban soil layers and 21 reference soil layers that did not have measured values, while measured K_s values for retained for 2690 records (1876 reference and 814 urban soil layers).

To estimate water retention parameters, data were compiled from 1871 samples in the National Cooperative Soil Survey database (NCSS, 2019). The first step required estimating van Genuchten (1980) model parameters (θ_r, θ_s, α, and m) for each sample based on measured water contents at 0 cm, -60 cm, -100 cm, -330 cm, and -15,000 cm. The optimal water retention parameters for each sample were fit using a Markov chain Monte Carlo (MCMC) approach. We then used random forest modeling to analyze the relationship between water retention parameters, soil textural components (i.e., percent sand, silt, and clay), categorical soil texture, bulk density, and soil water contents at -330 cm and -15,000 cm. Due to input data disparities, we ultimately developed four different random forest models for each van Genuchten parameter, each using one of the following sets of inputs: 1) categorical soil texture; 2) percent sand, silt, and clay (Figure B2); 3) percent sand, silt, and clay and bulk density; and 4) percent sand, silt, and clay, bulk density, and water contents at -330 and -15,000 cm. The reference profiles had 127 layers analyzed using the first PTF model (soil texture) and 1773 layers that were analyzed using the fourth PTF model (percent sand, silt, and clay, bulk density, and water contents at -330 and -15,000 cm). The urban profiles had 1830 records that were analyzed using the first PTF model, 701 record analyzed using the second PTF (percent sand, silt, and clay), and 70 records analyzed using the third PTF (percent sand, silt, and clay plus bulk density).

Appendix Caption

Appendix A – Alternative approximation for time to ponding
Appendix B – Development of pedotransfer functions

References

Bartlett MS, Parolari AJ, McDonnell JJ, Porporato A. 2016. Framework for event-based semidistributed modeling that unifies the SCS-CN method, VIC, PDM, and TOPMODEL. Water Resources Research, **52**: 7036-7056. DOI: 10.1002/2016wr019084.

Baruch EM, Voss KA, Blaszczak JR, Delesantro J, Urban DL, Bernhardt ES. 2018. Not all pavements lead to streams: variation in impervious surface connectivity affects urban stream ecosystems. Freshwater Science, **37**: 673-684.

Batey T. 2009. Soil compaction and soil management–a review. Soil use and management, **25**: 335-345.

Bonnin GM, Martin D, Lin B, Parzybok T, Yekta M, Riley D. 2006. Precipitation-frequency atlas of the United States. NOAA atlas, **14**: 1-65.

Bos M. 1994. Basics of groundwater flow. In: Drainage Principles and Applications, Ritzema HP (ed.) International Institute for Land Reclamation and Improvement, pp: 225-261.

Chen L, Young MH. 2006. Green-Ampt infiltration model for sloping surfaces. Water Resources Research, **42**. DOI: 10.1029/2005wr004468.

Dunkerley D. 2016. An approach to analysing plot scale infiltration and runoff responses to rainfall of fluctuating intensity. Hydrological Processes, **31**: 191-206. DOI: 10.1002/hyp.10990.

Dunkerley D. 2018. How is overland flow produced under intermittent rain? An analysis using plot-scale rainfall simulation on dryland soils. Journal of Hydrology, **556**: 119-130. DOI: 10.1016/j.jhydrol.2017.11.003.

Dunne T, Black RD. 1970. Partial area contributions to storm runoff in a small New England watershed. Water Resources Research, **6**: 1296-1311.

Fok Y-S. 1975. A comparison of the Green-Ampt and Philip two-term infiltration equations. Transactions of the ASAE, **18**: 1073-1075.

Freeze RA. 1974. Streamflow generation. Reviews of Geophysics, **12**: 627-647.

Gill SE, Handley JF, Ennos AR, Pauleit S. 2007. Adapting cities for climate change: the role of the green infrastructure. Built environment, **33**: 115-133.

Green WH, Ampt G. 1911. Studies on soil physics. Journal of Agricultural Science, **4**: 1-24.

Herrmann DL, Schifman LA, Shuster WD. 2018. Widespread loss of intermediate soil horizons in urban landscapes. Proceedings of the National Academy of Sciences, **115**: 6751-6755. DOI: 10.1073/pnas.1800305115.

Hopkins KG, Morse NB, Bain DJ, Bettez ND, Grimm NB, Morse JL, Palta MM, Shuster WD, Bratt AR, Suchy AK. 2015. Assessment of regional variation in streamflow responses to urbanization and the persistence of physiography. Environmental science & technology, **49**: 2724-2732.

Horton RE. 1933. The role of infiltration in the hydrologic cycle. Eos, Transactions American Geophysical Union, **14**: 446-460.

Kottek M, Grieser J, Beck C, Rudolf B, Rubel F. 2006. World map of the Köppen-Geiger climate classification updated. Meteorologische Zeitschrift, **15**: 259-263.

Leopold LB. 1968. Hydrology for urban land planning: A guidebook on the hydrologic effects of urban land use. US Department of the Interior, Geological Survey, **554**: 1-18.

Lim TC. 2016. Predictors of urban variable source area: a cross-sectional analysis of urbanized catchments in the United States. Hydrological Processes, **30**: 4799-4814. DOI: 10.1002/hyp.10943.

Loague K, Heppner CS, Ebel BA, VanderKwaak JE. 2010. The quixotic search for a comprehensive understanding of hydrologic response at the surface: Horton, Dunne, Dunton, and the role of concept- development simulation. Hydrological Processes, **24**: 2499-2505.

Masselink RJH, Heckmann T, Temme AJAM, Anders NS, Gooren HPA, Keesstra SD. 2016. A network theory approach for a better understanding of overland flow connectivity. Hydrological Processes, **31**: 207-220. DOI: 10.1002/hyp.10993.

McDonnell JJ. 2003. Where does water go when it rains? Moving beyond the variable source area concept of rainfall-runoff response. Hydrological Processes, **17**: 1869-1875.

McDonnell JJ. 2013. Are all runoff processes the same? Hydrological Processes, **27**: 4103-4111. DOI: 10.1002/hyp.10076.

Miles B, Band LE. 2015. Green infrastructure stormwater management at the watershed scale: urban variable source area and watershed capacitance. Hydrological Processes, **29**: 2268-2274. DOI: 10.1002/hyp.10448.

Miller JF, Frederick RH, Tracey RJ. 1973. Precipitation-frequency atlas of the western United States.

Morel-Seytoux HJ, Meyer PD, Nachabe M, Touma J, van Genuchten MT, Lenhard RJ. 1996. Parameter equivalence for the Brooks-Corey and van Genuchten soil characteristics: Preserving the effective capillary drive. Water Resources Research, **32**: 1251-1258. DOI: 10.1029/96WR00069.

NCSS. 2019. National Cooperative Soil Survey Characterization Database. United States Department of Agriculture Natural Resources Conservation Service.

Niyogi D, Lei M, Kishtawal C, Schmid P, Shepherd M. 2017. Urbanization impacts on the summer heavy rainfall climatology over the eastern United States. Earth Interactions, **21**: 1-17.

Oosterbaan R, Nijland H. 1994. Determining the Saturated Hydraulic Conductivity. In: Drainage Principles and Applications, Ritzema HP (ed.) International Institute for Land Reclamation and Improvement, pp: 435-476.

Philip JR. 1969. Theory of infiltration. In: Advances in Hydroscience, Chow VT (ed.), pp: 215-296.

Schifman LA, Herrmann DL, Shuster WD, Ossola A, Garmestani A, Hopton ME. 2017. Situating Green Infrastructure in Context: A Framework for Adaptive Socio-Hydrology in Cities. Water Resources Research, **53**: 10139-10154. DOI: 10.1002/2017wr020926.

Schifman LA, Shuster WD. 2018. Comparison of Measured and Simulated Urban Soil Hydrologic Properties. Journal of Hydrologic Engineering, **24**: 04018056.

Schifman LA, Tryby ME, Berner J, Shuster WD. 2018. Managing Uncertainty in Runoff Estimation with the US Environmental Protection Agency National Stormwater Calculator. JAWRA Journal of the American Water Resources Association, **54**: 148-159.

Schwartz SS, Smith B. 2016. Restoring hydrologic function in urban landscapes with suburban subsoiling. Journal of Hydrology, **543**: 770-781. DOI: 10.1016/j.jhydrol.2016.10.051.

Selker J, Assouline S. 2017. An explicit, parsimonious, and accurate estimate for ponded infiltration into soils using the Green and Ampt Approach. Water Resources Research, **53**: 7481-7487. DOI: 10.1002/2017wr021020.

Shuster WD, Bonta J, Thurston H, Warnemuende E, Smith D. 2005. Impacts of impervious surface on watershed hydrology: A review. Urban Water Journal, **2**: 263-275.

Shuster WD, Dadio S, Drohan P, Losco R, Shaffer J. 2014. Residential demolition and its impact on vacant lot hydrology: Implications for the management of stormwater and sewer system overflows. Landscape and Urban Planning, **125**: 48-56.

Shuster WD, Dadio SD, Burkman CE, Earl SR, Hall SJ. 2015. Hydropedological Assessments of Parcel-Level Infiltration in an Arid Urban Ecosystem. Soil Science Society of America Journal, **79**: 398-406. DOI: 10.2136/sssaj2014.05.0200.

Smith BK, Smith JA. 2015. The flashiest watersheds in the contiguous United States. Journal of Hydrometeorology, **16**: 2365-2381.

Soil Survey Staff. 2014. Keys to soil taxonomy, 12th edn. USDA-NRCS. US Gov. Print. Office, Washington, DC.

Stewart RD. 2019. A Generalized Analytical Solution for Preferential Infiltration and Wetting. Vadose Zone Journal, **18**. DOI: 10.2136/vzj2018.08.0148.

Stewart RD, Abou Najm MR. 2018. A comprehensive model for single ring infiltration. 1: Influence of initial water content and soil hydraulic properties. Soil Science Society of America Journal, **82**: 548-557. DOI: 10.2136/sssaj2017.09.0314.

Stewart RD, Rupp DE, Najm MRA, Selker JS. 2013. Modeling effect of initial soil moisture on sorptivity and infiltration. Water Resources Research, **49**: 7037-7047. DOI: 10.1002/wrcr.20508.

Thomas SK, Conta JF, Severson ED, Galbraith JM. 2016. Measuring Saturated Hydraulic Conductivity in Soil. Virginia Cooperative Extension, pp: 1-13.

Tzoulas K, Korpela K, Venn S, Yli-Pelkonen V, Kaźmierczak A, Niemela J, James P. 2007. Promoting ecosystem and human health in urban areas using Green Infrastructure: A literature review. Landscape and urban planning, **81**: 167-178.

U.S. E.P.A. 2013. On the Road to Reuse: Residential Demolition Bid Specification Development Tool.

van Genuchten MT. 1980. A closed-form equation for predicting the hydraulic conductivity of unsaturated soils. Soil Science Society of America Journal, **44**: 892-898. DOI: 10.2136/sssaj1980.03615995004400050002x.

Voter C, Loheide S. 2018. Urban Residential Surface and Subsurface Hydrology: Synergistic Effects of Low- Impact Features at the Parcel Scale. Water Resources Research, **54**: 8216-8233.

Yang W-Y, Li D, Sun T, Ni G-H. 2015. Saturation-excess and infiltration-excess runoff on green roofs. Ecological Engineering, **74**: 327-336. DOI: 10.1016/j.ecoleng.2014.10.023.

Zangar CN. 1953. Theory and problems of water percolation. U.S. Bureau of Reclamation.

Zhang R. 1997. Infiltration models for the disk infiltrometer. Soil Science Society of America Journal, **61**: 1597-1603.

Zimmer MA, McGlynn BL. 2018. Lateral, Vertical, and Longitudinal Source Area Connectivity Drive Runoff and Carbon Export Across Watershed Scales. Water Resources Research, **54**: 1576-1598. DOI: 10.1002/2017wr021718.

Tables

Table 1. Assignment of values to variables *a* and *b* for infiltration-excess overland flow (IEOF) and saturation-excess overland flow (SEOF) conditions, based on Equations (19), (20), and (21).

	IEOF	SEOF
a	$\frac{\tau-\tau_p}{\tau}$	1
b	$1+\frac{\tau}{\tau-\tau_p}\ln\left(\frac{1+A\tau+\sqrt{2\tau}}{1+A\tau_p+\sqrt{2\tau_p}}\right)$	$\left(\frac{Z}{h_f\tau}\right)$

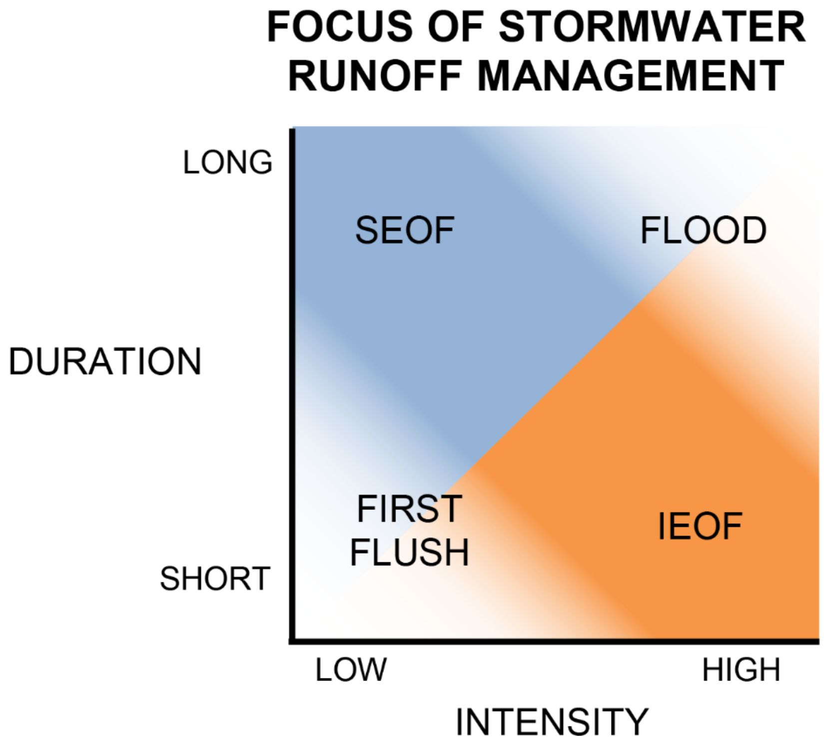

Figure 1. Stormwater runoff management may have different emphasis based on the intensity versus duration of precipitation events. Low intensity, short duration storms may cause first flush mobilization of deposited pollutants, while high intensity, long duration storms may caues flood conditions that overwhelm the potential capacity of urban soils to infiltrate and store water. For all other cases, stormwater management will depend on whether surface runoff is generated via infiltration-excess overland flow (IEOF) or saturation-excess overland flow (SEOF).

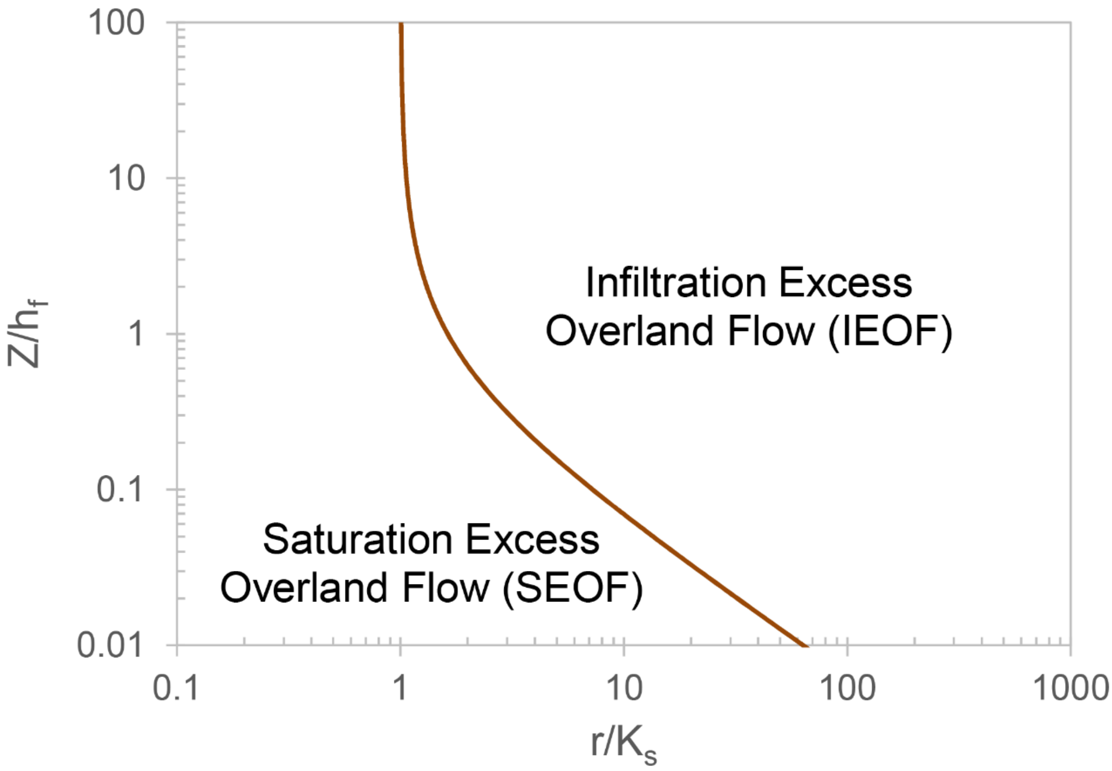

Figure 2. Delineation of conditions that favor IEOF versus SEOF, as quantified by Equation (7) assuming $B = 5/8$. r/K_s represents the non-dimensional ratio of precipitation rate to saturated hydraulic conductivity, and Z/h_f represents the non-dimensional ratio of soil profile depth to wetting front potential.

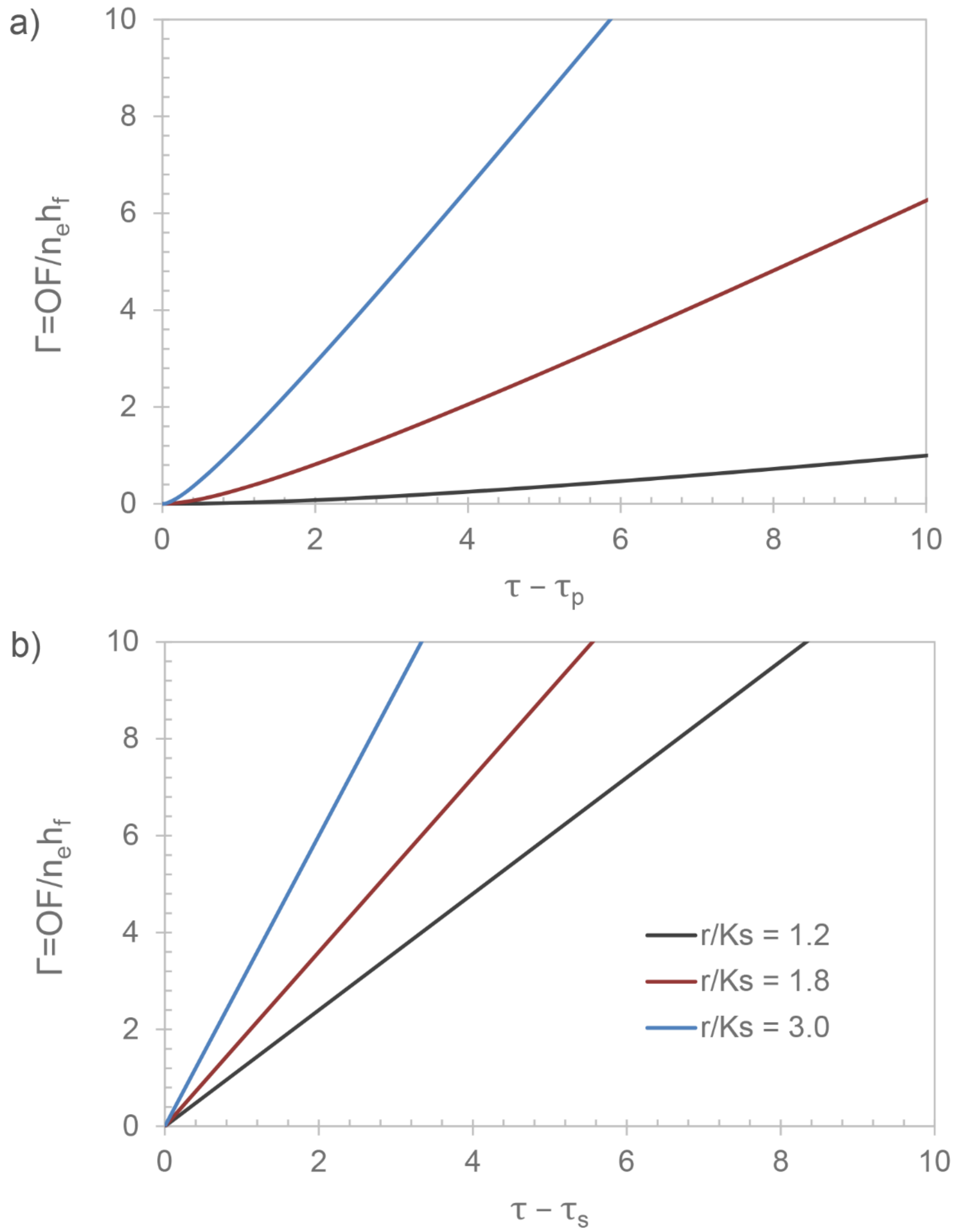

Figure 3. Non-dimensional overland flow depth Γ versus non-dimensional time, τ, for a) IEOF, and b) SEOF, shown here for r/K_s values of 1.2, 1.8, and 3.

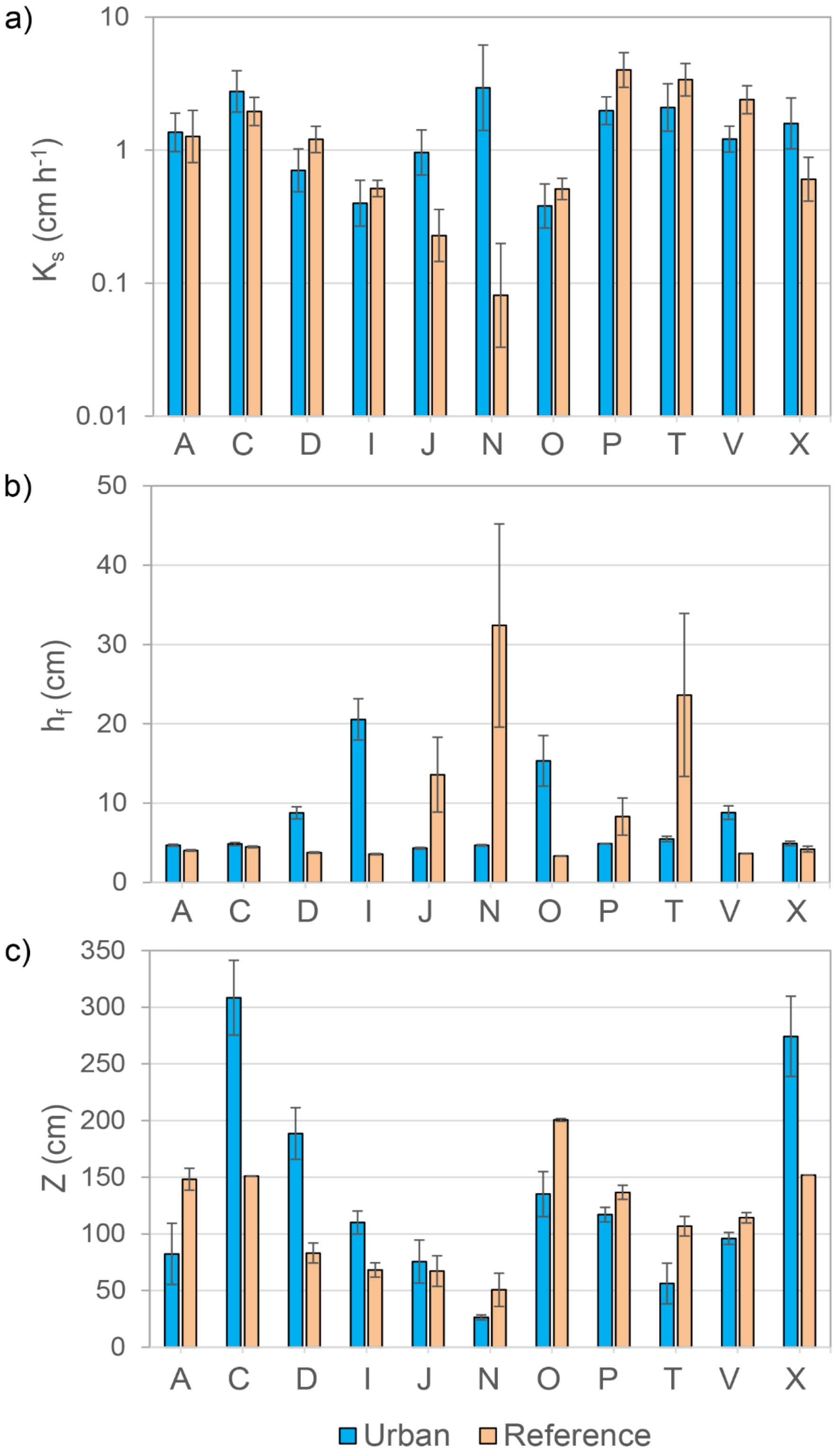

Figure 4. Per-city mean values of a) K_s, b) h_f, and c) Z for reference and urban profiles. K_s values are presented as geometric means ± 95% confidence intervals; h_f and Z values are presented as arithmetic means ± standard errors of the means. A = Atlanta, GA; C = Camden, NJ; D = Detroit, MI; I = Cincinnati, OH; J = San Juan, PR; N = New Orleans, LA; O = Omaha, NE; P = Portland, ME; T = Tacoma, WA; V = Cleveland, OH; X = Phoenix, AZ. *'s indicate significant differences between urban and reference values (pairwise t-test; $p < 0.05$).

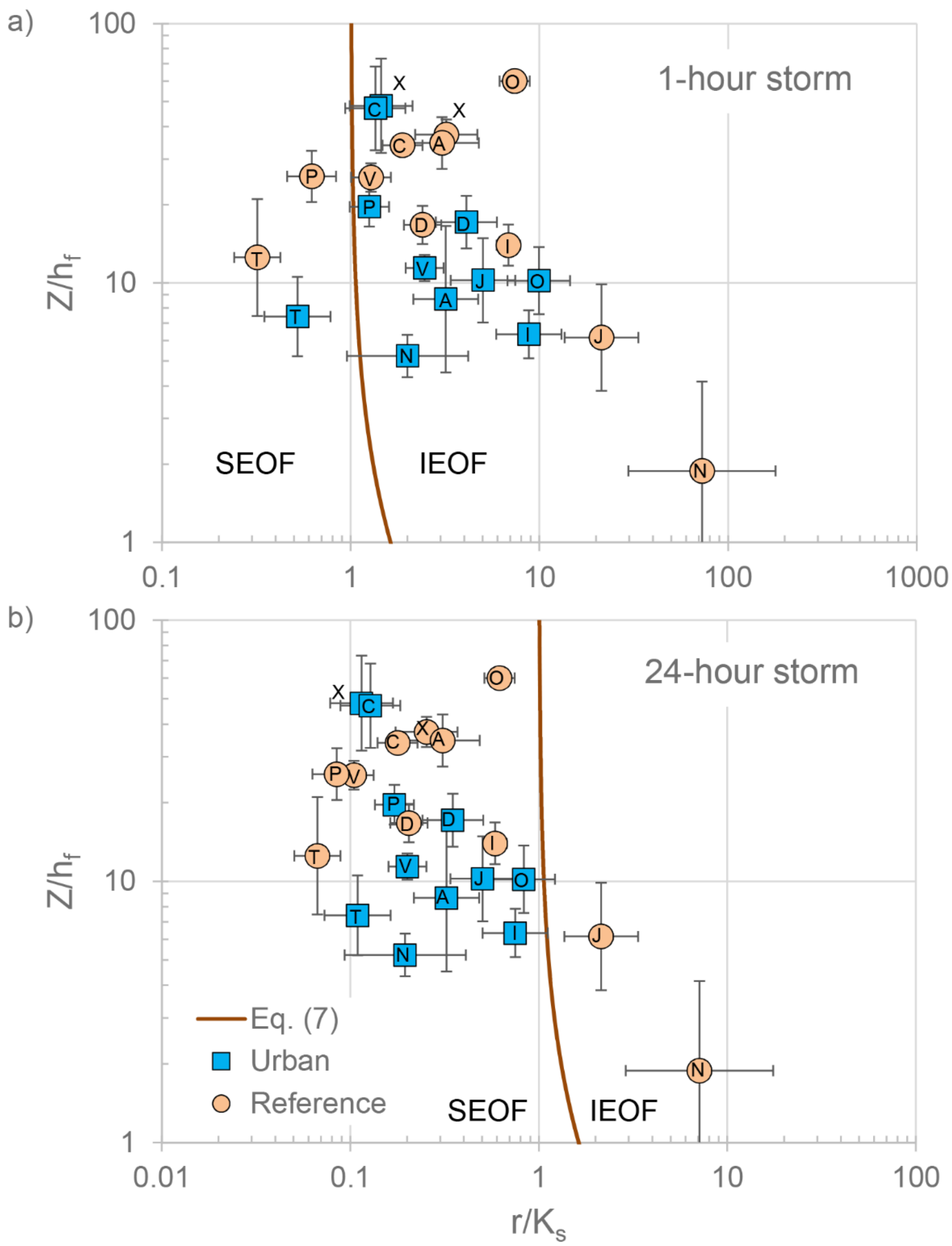

Figure 5. Non-dimensional hydraulic characteristics (Z/h_f versus r/K_s) of 11 U.S. cities for a) 1-hour and b) 24-hour storms with 2-year recurrence intervals. Note shift in x-axis scaling. Points indicate geometric mean values; error bars indicate 95% confidence intervals. Eq. (7) was applied assuming B = 5/8. A = Atlanta, GA; C = Camden, NJ; D = Detroit, MI; I = Cincinnati, OH; J = San Juan, PR; N = New Orleans, LA; O = Omaha, NE; P = Portland, ME; T = Tacoma, WA; V = Cleveland, OH; X = Phoenix, AZ.

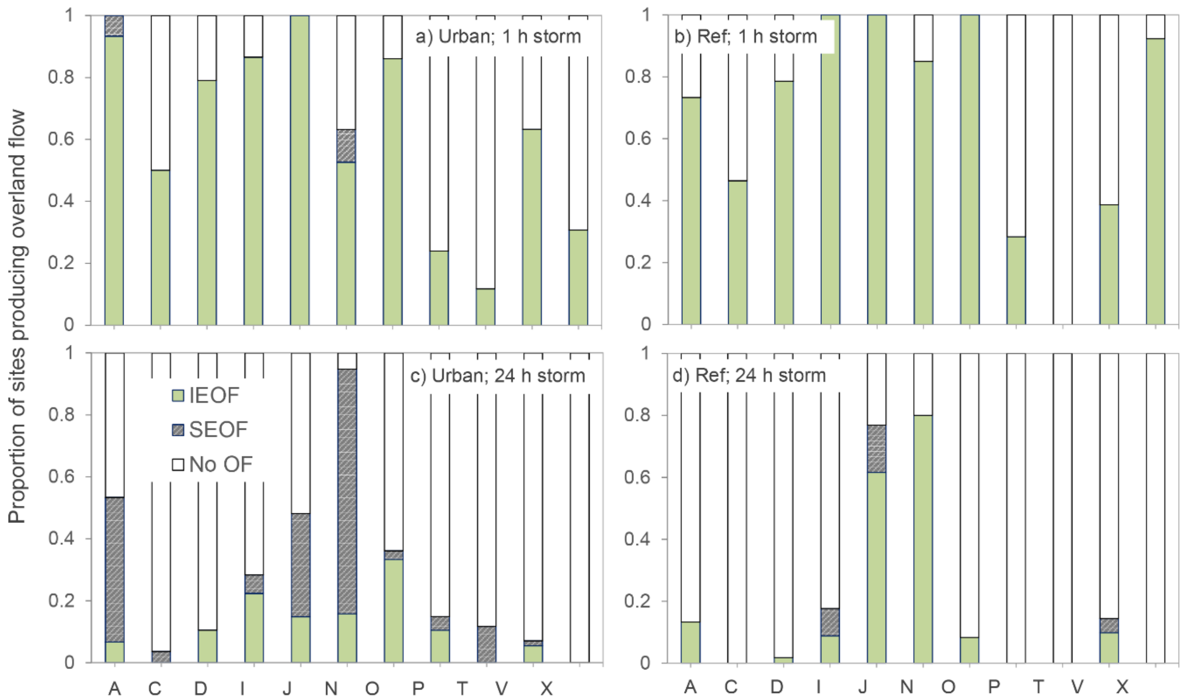

Figure 6. Proportion of profiles in each city that produce overland flow, and whether that generation was through IEOF or SEOF. Profiles that did not produce overland flow are labeled "No OF". Panels a) and b) show 1-hour, 2-year storms, while c) and d) show 24-hour, 2-year storms. Panels a) and c) show post-development profiles ("Urban"); b) and d) show pre-development reference profiles ("Ref"). A = Atlanta, GA; C = Camden, NJ; D = Detroit, MI; I = Cincinnati, OH; J = San Juan, PR; N = New Orleans, LA; O = Omaha, NE; P = Portland, ME; T = Tacoma, WA; V = Cleveland, OH; X = Phoenix, AZ.

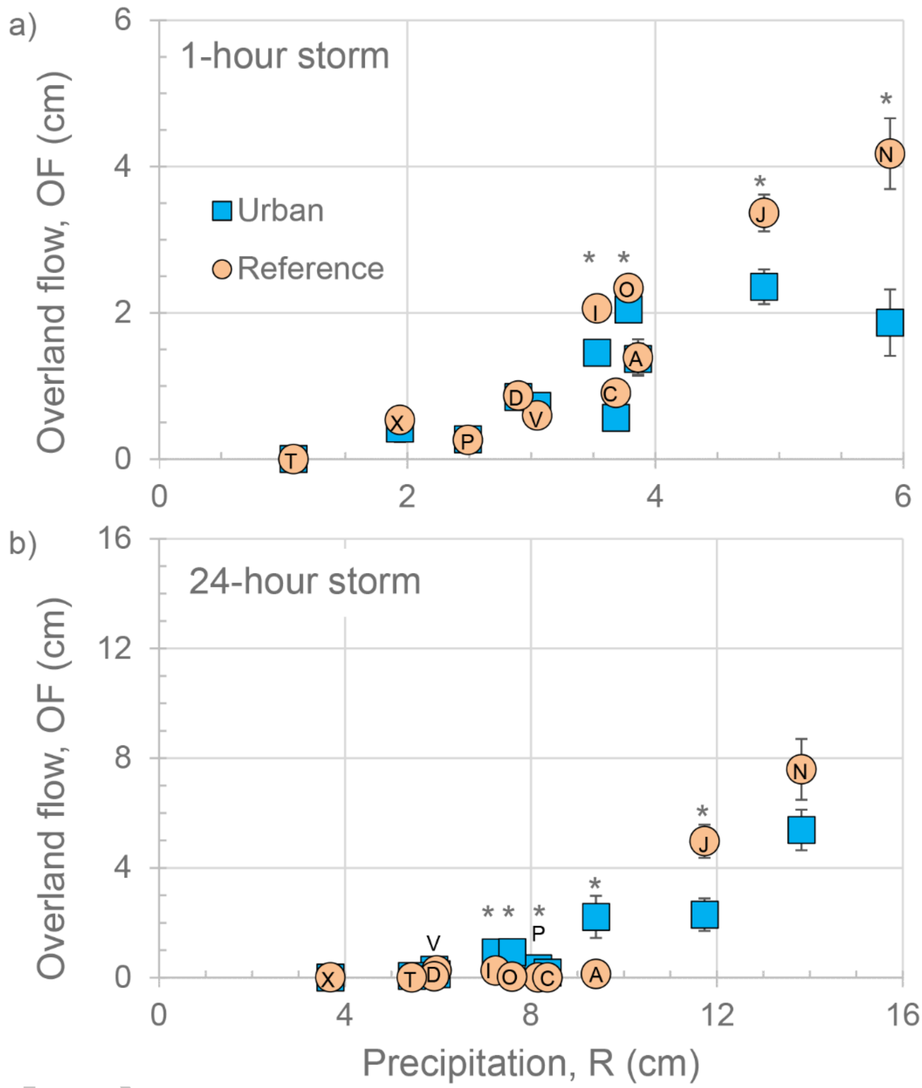

Figure 7. Estimations of cumulative overland flow, OF (cm), based on cumulative precipitation, R (cm), for a) 1-hour and b) 24-hour storms with 2-year recurrence intervals. Urban represents measured values after urbanization; reference indicates pre-development characteristics. Points indicate mean values; error bars indicate standard errors of the mean. A = Atlanta, GA; C = Camden, NJ; D = Detroit, MI; I = Cincinnati, OH; J = San Juan, PR; N = New Orleans, LA; O = Omaha, NE; P = Portland, ME; T = Tacoma, WA; V = Cleveland, OH; X = Phoenix, AZ. *'s indicate significant differences between urban and reference values (pairwise t-test; $p < 0.05$).

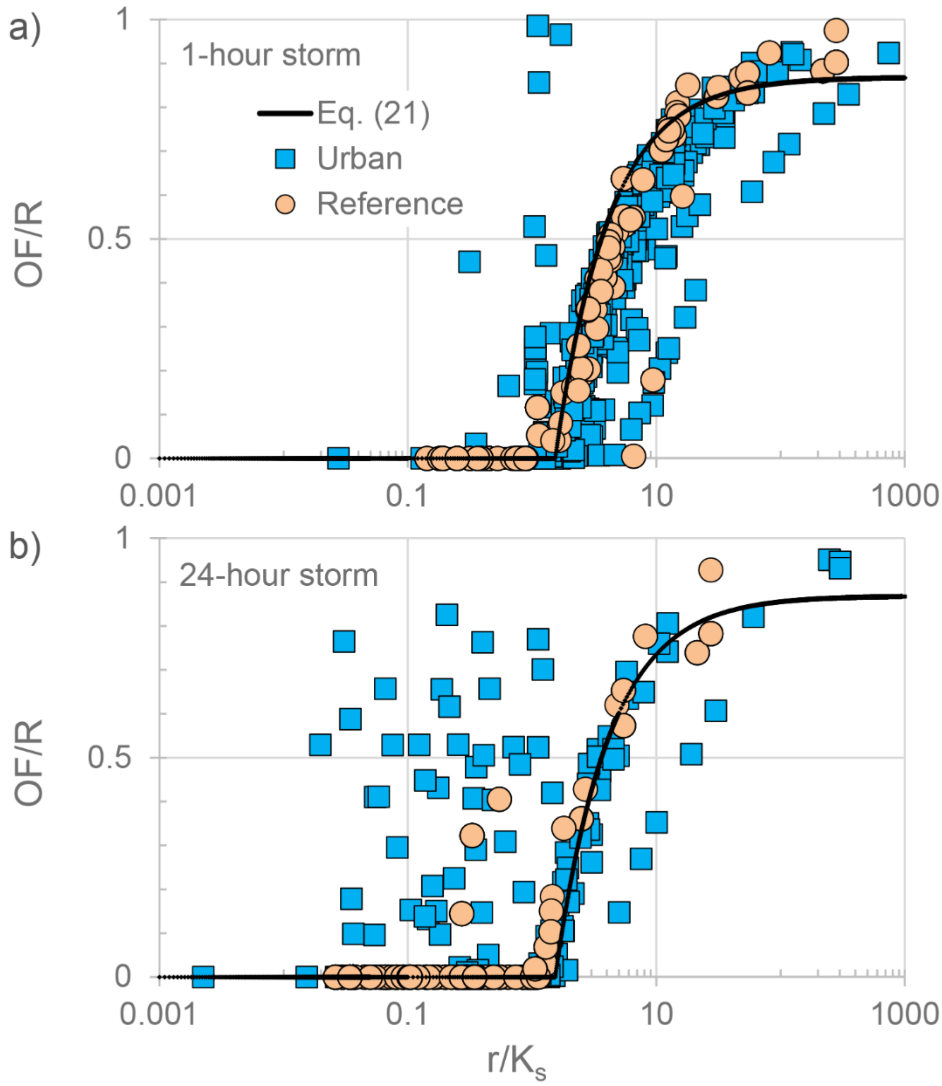

Figure 8. Runoff ratio (*OF*/*R*) as a function of r/K_s, with *r* estimated using a) a 1-hour, 2-year storm, and b) a 24-hour, 2-year storm. Urban represents measured values after urbanization; Reference indicates pre-development characteristics. Equation (21) was plotted using mean values for *a* and *b* based on all samples (*a* = 0.869; *b* = 1.53).

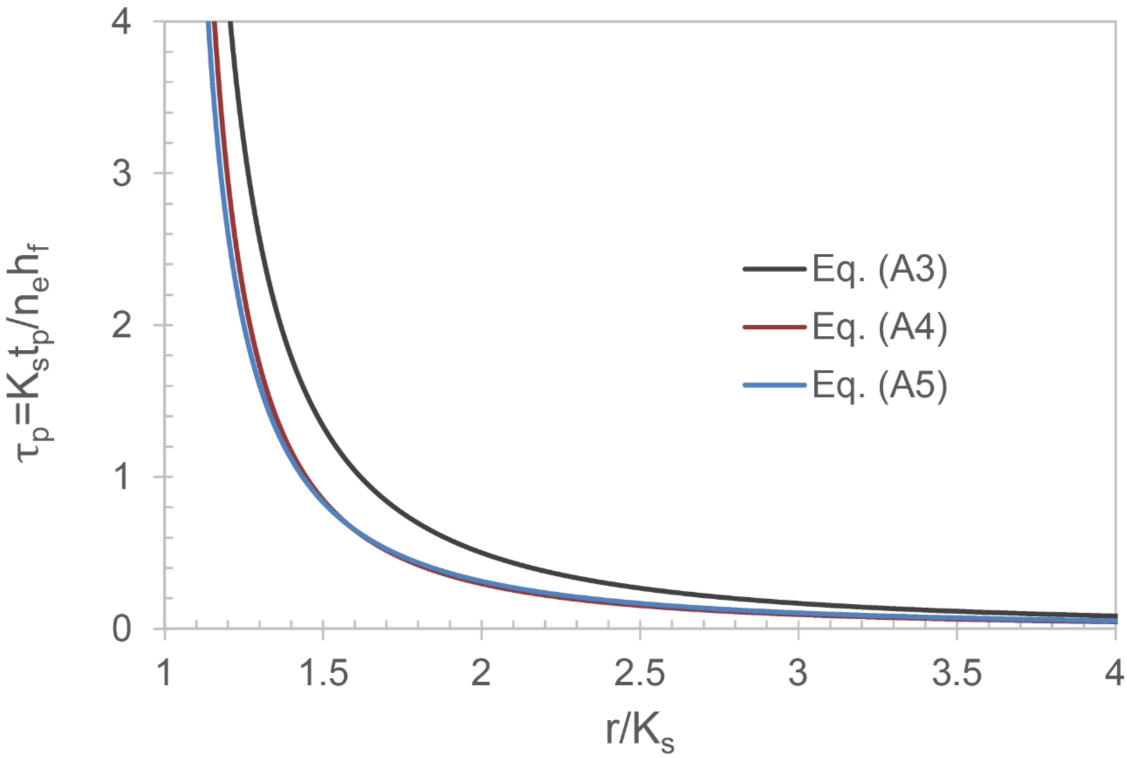

Figure A1. Estimated normalized time to ponding as a function of relative precipitation rate for three models. Equation (A4) was plotted with $A = 2/3$ and Equation (A5) was plotted with $B = 5/8$.

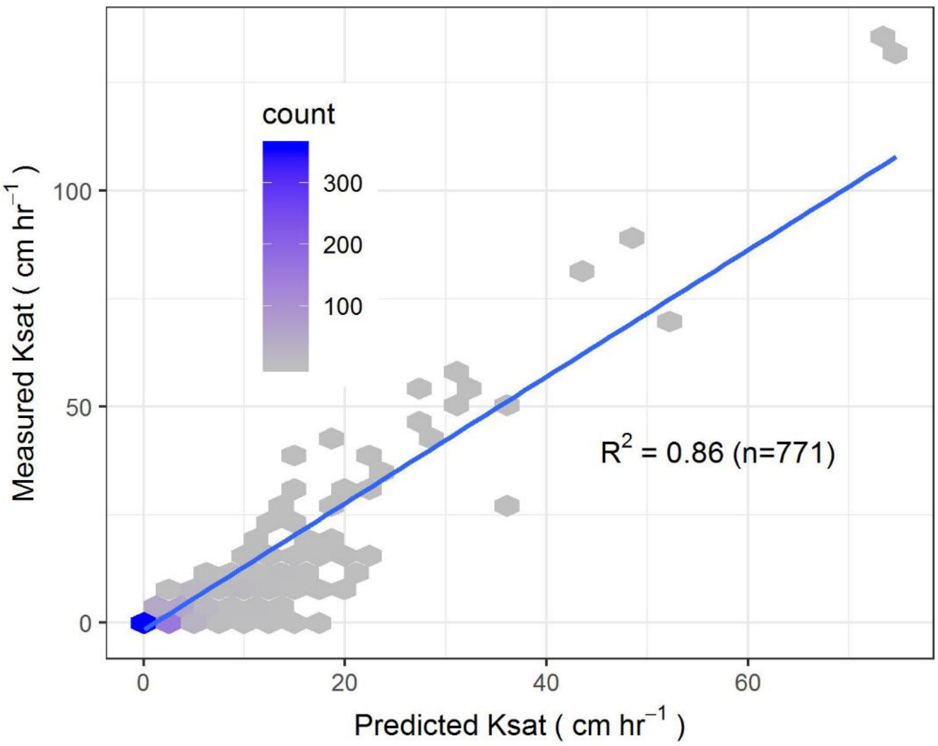

Figure B1. K_s predicted using the random forest pedotransfer function (PTF) developed in this study versus measured K_s values. Input data for the PTF model are percent sand, silt, and clay; the blue line indicates linear regression results.

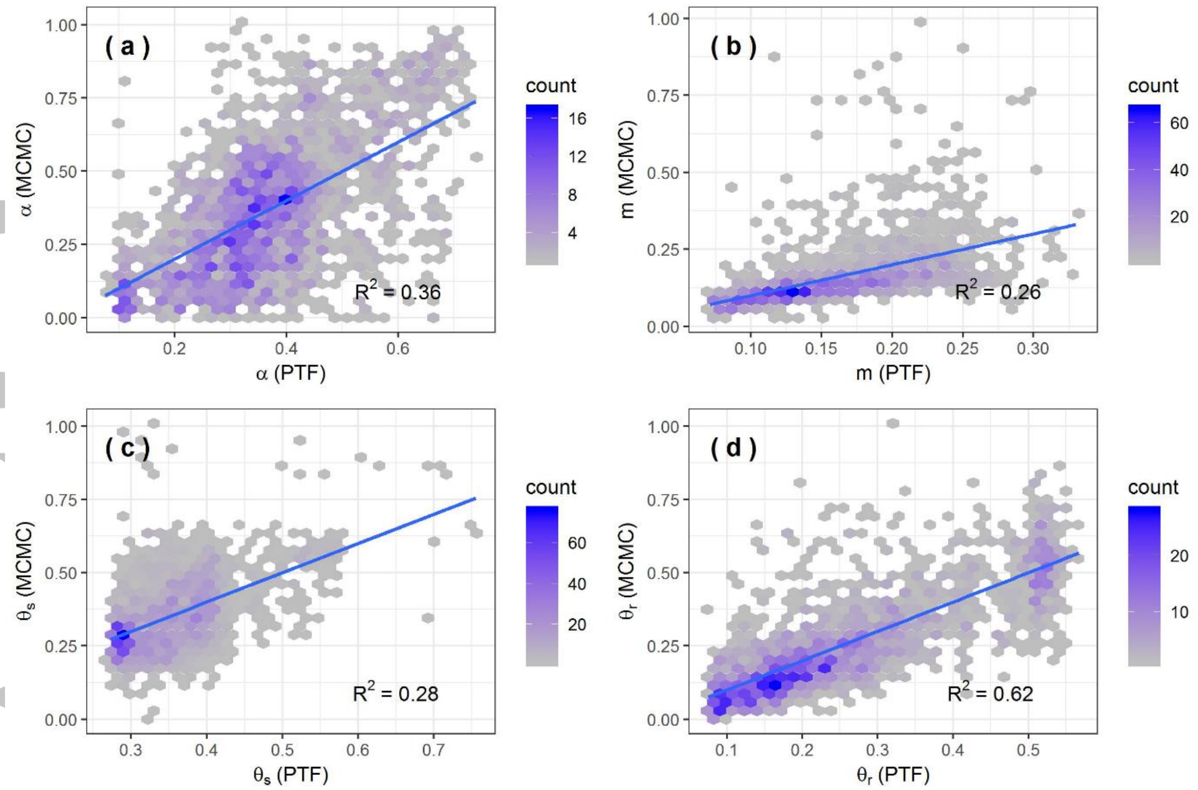

Figure B2. Predicted parameters using a random forest (RF) model for the van Genuchten (1980) water retention parameters – a) α, b) m, c) θ_r, and d) θ_s – versus parameter values that were constrained from measured data using a Markov chain Monte Carlo (MCMC) approach. Input data for the PTF model are percent sand, silt, and clay; the blue lines indicate linear regression results.